HHS Public Access

Author manuscript

Int J Oral Maxillofac Implants. Author manuscript; available in PMC 2014 August 11.

Published in final edited form as:

Int J Oral Maxillofac Implants. 2013 ; 28(6): 1581–1588.

Quantitative Percussion Diagnostics and Bone Density Analysis of the Implant-Bone Interface in a Pre- and Postmortem Human Subject

Cherilyn G. Sheets, DDS[1] **[Co-Executive Director]**, **DiDi Hui, BS**[2], **Vaibhav Bajaj, BS**[3], and **James C. Earthman, PhD**[4] **[Biomedical Engineering Professor]**

[1]Newport Coast Oral-Facial Institute, 360 San Miguel, Suite 204, Newport Beach, CA 92660 USA, cgsheets@ncofi.org, Telephone: 949-760-6288, Fax: 949-760-5048

[2]Department of Biomedical Engineering, The Henry Samueli School of Engineering, University of California, Irvine, CA 92697-2575 USA

[3]Department of Biomedical Engineering, University of California, San Diego, La Jolla, CA 92093-0403

[4]Department of Chemical Engineering & Materials Science The Henry Samueli School of Engineering University of California, Irvine, CA 92697-2575 USA

Abstract

Purpose—It has been hypothesized that a correlation exists between the density of surrounding cortical bone and the stability of an implant under percussion loading that can be used to quantify the implant's osseointegration. The purpose of the present research was to explore whether quantitative percussion testing of dental implants gives reasonable indications of the level of osseointegration that are consistent with bone configuration and its influence on osseointegration quality.

Material and Methods—Data from percussion testing of a live human subject, obtained using the Periometer®, were compared with corresponding bone density estimates from high-resolution computer tomography images and postmortem percussion probe data.

Results—The results confirm the hypothesis that the nature of an implant’s response to percussion is determined by its cortical bone support.

Conclusions—The findings suggest that the cortical bone supporting the crestal and apical regions of the implant is primarily responsible for structural stability.

Keywords

alveolar bone; bone loss; computed tomography; dental implants; osseointegration; technology

Correspondence to: Cherilyn G. Sheets.

Introduction

Osseointegration is a long-term, direct structural and functional connection between bone and an implant.[1,2] The durability of an implant depends on how well it can integrate with the bone, providing stability that can withstand loads and stresses exerted by external impacts and prolonged parafunctional loading. It has become clear that a quantifiable system to assess the quality/quantity of bone support for a dental implant could help clinicians more accurately plan treatment based on structural stability data.[3–6] Quantifiable measurements could expand the current implant "success" or "failure" approach that is generally accepted by the profession. Greater precision in assessing "success" would allow the rating of implants regarding their strength and ability to accept loads in a more biomechanically designed treatment plan. More complete knowledge of how a given implant responds to mechanical loading may also allow clinicians to make more appropriate restorative material choices to complement the strength or weakness of the osseointegrated dental implant when surrounded by natural teeth of varying stabilities.[7–10]

Percussion testing is a physiologic method that can provide relevant data regarding the mechanical behavior and structural stability of a biologic system. It has been used qualitatively for many years in medicine and dentistry for the diagnosis of abnormalities in joints, organs, tissues, and teeth.[11–13] The Periometer® (Perimetrics LLC) is a percussion probe diagnostic instrument that records and analyzes the percussion response of implant structures and teeth. This instrument provides two important assessment quantities: the loss coefficient, which indicates overall implant or tooth stability, and the normal fit error (NFE), which was derived to characterize local instabilities in the structure.[14–18] A description of how NFE is determined is given in Appendix A.[19]

One method to determine the degree of osseointegration is x-ray computed tomography (CT). This technique can be used to assess relative bone density surrounding an implant, since absorption of x-rays is directly associated with bone density.[20–23] This relationship provides an opportunity to evaluate the quality of bone surrounding implant if radiation scatter can be controlled by removing metallic restorative components.[24,25] Additionally, cadaver subjects offer the possibility of using higher radiation levels to provide enhanced-resolution images of the bone supporting implant.[26]

The goal of the present work was to determine whether high-resolution CT data for a cadaver subject could be correlated to the measured percussion response provided by the Periometer. This research was motivated by the hypothesis that the percussion response can be used to diagnose the structural integrity of the surrounding bone that supports an implant. In this work, percussion results were compared to relative bone density assessments determined from high-resolution CT scans of a subject's mandible and maxilla.

Materials and Methods

Human subject JS received full-mouth mechanical percussion testing over multiple years as an Institutional Review Board-approved research patient to study percussion probe diagnostics in teeth and dental implants. When the subject died, the subject's body was

donated to the Willed Body Program at the University of California at Irvine. The gold milled abutments and porcelain-fused-to-gold superstructures were removed prior to scanning to eliminate radiation scatter caused by the gold. There was no radiation scatter noted from the titanium implants. High-resolution CT images were obtained from the cadaver, allowing for detailed analysis of the bony support surrounding the osseointegrated and clinically successful dental implants in the maxilla and mandible.

The present work investigated the bone density surrounding all 11 dental implants in human subject cadaver JS. The CT data analyzed in the present work were generated using the Flash CT 2252 system (Hytec Imaging). The specimen jaws were scanned in air at the highest radiation levels possible for this system (peak x-ray tube potential = 420 kV and x-ray intensity = 5,300 **μ**A) to provide maximum contrast and consistency between samples. The data were formatted at Stanford University under the guidance of Dr. Eric Herbranson. Data were subsequently returned to the School of Engineering, University of California at Irvine, for further analysis. The voxel size of the three-dimensional CT images are 100 **μ**m in the maxilla and 200 **μ**m in the mandible.[27] The maxillary implants were located in the right first and second molar, right canine, left lateral incisor, left first premolar, and left first molar areas; and the mandibular implants were located in the left first and second molar, left first premolar, right second premolar, and right first molar areas. The following analysis of bony support was performed from the raw CT data with full opacity of the pixels. In Fig 1, the inferior border of the mandible with pixels having grayscale of 35,150 intensity is highlighted in red to demonstrate that any grayscale at 35,150 and higher is representative of known areas of high-density cortical bone.

Image J image analysis software (National Institutes of Health) was used to analyze two-dimensional CT slices to determine the relative bone density along the implant-bone interfaces. Five equidistant positions, from the bony crest to the apex of the implant, were selected by CT image slice number for further analysis. Histograms were compiled using Image J that included only pixels corresponding to the 2 mm of bone surrounding the implants. The pixels corresponding to the implants were segmented from the bone tissue so that they would not affect the bone tissue analysis.[28] In each slice, the grayscale varied in range from 32,000 to 40,000; lower numbers corresponded to the darker grayscale shades, inferring lower-density bone or no bone at all, and the higher-grayscale numbers corresponded to denser bone.

The relative mean bone density, defined as the average grayscale shade for the present work, was determined for the five aforementioned evenly spaced CT slices along the length of each implant. For each CT slice along an implant, a mode for the high-density cortical bone was also recorded, defined as the number of pixels with a grayscale value of 35,150 and above. Thus, three-dimensional information for each implant was obtained, albeit from five specific vertical locations. With these specific locations it was possible to determine how the cortical bone in the specific areas affected the stability of the implant according to the percussion results.

Several approaches were used to investigate the correlation between the percussion probe data and the stability of the implant. The first approach was to simply compare the average

relative bone density to the NFE. The second approach was performed by calculating the average percent cortical bone for all six slices of each implant and comparing the results to the NFE. The final approach was attained by calculating the average percent cortical bone of solely the crestal and apical slices of each implant and comparing it to the NFE.

Results

Fig 2 shows the specific CT scans of the bone surrounding four of the implants (sites: maxillary right first premolar, maxillary left lateral incisor, mandibular left first premolar, and mandibular right first molar) at the crestal bone level. The red fields signify the densest cortical bone surrounding the implant. Histograms at the bony crest of the same implant sites display the grayscale 35,150 and higher (Fig 2). For example, as shown in the histograms, the mandibular right first molar and mandibular left first premolar sites had a significantly higher amount of cortical bone above 30%, as compared to the maxillary sites, which had less than 6% cortical bone at the crest of the implants.

A plot of the NFE vs. average relative bone density is presented in Fig 3. Overall, the data followed a general trend of decreasing bone density with increasing NFE. However, the correlation coefficient, *R*, for a linear regression fit to the data was found to be relatively low at 0.341. Additionally, the Student *t* test of the null hyposthesis (H_0: r = 0) produced a *P* value of .305, indicating that the observed correlation between the average relative bone density and NFE was not statistically significant.

It was also determined that each of the 11 implants fell into one of four different bony support categories. These categories included sites with high-density crestal and apical bone (mandibular right first molar #46); sites with high-density crestal bone but low-density apical bone (mandibular left first premolar #34, mandibular right second premolar, #45); sites with low-density crestal bone but high-density apical bone (maxillary right first premolar, #14, and maxillary left first molar, #26); and finally sites with low-density crestal and apical bone maxillary right second premolar #15, maxillary right canine #13, maxillary left lateral incisor #22, maxillary left first premolar #24, mandibular left first and second molars, #36 and #37). Four implants were chosen to illustrate these four categories in the following discussions: sites 46 (mandibular right first molar), 34 (mandibular left first premolar), 14 (maxillary right first premolar), and 22 (maxillary left lateral incisor). These four implants provide a representative overview of potential osseointegration configurations.

Energy return data are shown for the four representative implants (sites 46, 34, 14, and 22) in Fig 4. The data for site 46 indicated a relatively high cortical bone density and presented a normal energy return response (Fig 4a). The NFE for this site was 0.008, a relatively low value that was consistent with the uniform shape of the data peak. A somewhat higher NFE of 0.019 at site 34 was recorded with percussion probe diagnostic testing of this site. In site 14, the small peak and associated extended time for the response dose led to a higher value of the NFE (0.021). The percussion diagnostic response for site 22 was distorted in terms of the shape of the energy return peak and in its longer overall duration on the x axis (Fig 4d). It was noted that the duration for site 22 extended beyond the small additional peak observed for site 14 (Fig 4c). The resulting NFE value for site 22 was 0.075, which was the highest

value among all 11 implants investigated in the present study. In addition to site 22 having the greatest NFE, it had lowest normalized energy return in the y-axis of all sites, confirming a lack of bone support.

Estimates of average amount of cortical bone at sites 14, 22, 34, and 46 were calculated from high-resolution CT data and plotted as a function of distance (from the crest to the apex) for five positions along the length of each implant (Fig 5). Site 46 exhibited an overall cortical bone level above 30% throughout the entire implant (Fig 5a). This finding suggests that there are no significant defects at the bone/implant interface and that the supporting bone is relatively dense. These findings agree well with the low NFE value determined from the corresponding percussion response data (Fig 4a).

A relatively low cortical bone percentage of 29.9% (< 30%) was observed near the apex of the implant at site 34 (Fig 5b). The cortical bone percentage was otherwise relatively high for this implant, particularly from the midpoint to the crest. It was noted that the percussion response (Fig 4b) had a longer duration than that for site 30, in addition to a higher NFE. It appears that the longer duration may be caused by the relatively low cortical bone density near the implant apex.

Figure 5c indicates a relatively low cortical bone percentage (less than 6%) near the crest of the implant at site 14. The apparent lack of cortical bone support near the crest is consistent with the irregularity observed in the response (plotted in Fig 4c) that resulted in a moderately high NFE value determined for the site. However, the denser cortical bone at the other test points along the length of the implant appeared to result in an otherwise stable percussion response.

Site 22 exhibited the lowest overall cortical bone of all of the sites in the present study (Fig 5d). In contrast to the sites discussed earlier, this site specifically exhibited weaker crestal and apical cortical bone support. This result from the CT data scans is also consistent with the percussion data, which were irregular in the shape of the peak (highest observed NFE value) and longest in duration (Fig 4d).

The percussion probe data describe the behavior of the implant response from percussion loading on the buccal side of the tooth. A schematic is shown in Fig 6 to describe the potential implant responses, which are dependent upon levels of bone support. Stable implant behavior is generally observed with percussion diagnostics when cortical bone support is present along the entire length of the implant. With relatively low levels of cortical bone (cancellous bone or voids) at either the crest or apex, a point of significant instability in the structure can be detected. Sites with low levels of cortical bone or voids at both the crest and the apex can cause substantially more detectable instability, as the implant has more freedom to pivot about the remaining bone support.

The average percent cortical bone was determined from five slices along the length of each implant. The resulting values are plotted as a function of NFE in Fig 7. The trend in the data indicated that as the percentage of cortical bone increased, NFE tended to decrease. This agrees with the concept that implants lacking good cortical bone are relatively unstable. The

correlation coefficient for a linear regression in this case is 0.581. A *P* value of 0.609 was obtained from the Student *t* test of the null hypothesis.

The average percent cortical bone of the crestal and apical slices of each implant is plotted in Fig 8 with respect to the NFE. The correlation coefficient in this plot is 0.736, which is greater than both *R* values exhibited in Figs 3 and 7. Moreover, the *P* value obtained from the Student *t* test of the null hypothesis was .0098, the lowest *P* value determined in the present study. Based on these data, the most significant correlation found in the present study was between the amount of crestal and apical cortical bone and the NFE.

Discussion

The better correlation of the data in Fig 8 suggests that the amount of dense cortical bone at the crest and at the apex is a more accurate determining factor of an implant's mechanical stability. This plot also indicates that the stability of implants potentially depends more on the amount of cortical bone support at the crestal and apical regions of the implant than the bone supporting the central portion of the implant.

Four representative implants (46, 34, 14, and 22) were discussed above to highlight the four basic stability categories discovered in the data analysis. The energy return curves and the average cortical bone plot determined from high-resolution CT of site 46 are shown in Figs 4a and 5a, respectively. These results convey that site 46 gave a normal response to percussion probe diagnostic testing and had a relativey high level of cortical bone support from crest to apex. This site is representative of a normal healthy osseointegrated implant. The stable crest and stable apex were also confirmed by the CT scan slices, which showed high levels of cortical bone support at the crest and apex, as depicted for the crestal bone in Fig 2a.

The energy return curves and the average cortical bone plot for site 34 in Figs 4b and 5b, respectively, showed that this sample was supported by a high level of cortical bone at the crest (stable crest) but by a decreased level of cortical bone at the apex (unstable apex). From the crestal CT scan slices in Fig 2b, it can been seen again that site 34 had a high level of cortical bone support near the crest (stable crest). The CT slices at the apex demonstrated a lower level of cortical bone support at the apex (unstable apex), consistent with the other findings. The implant at site 21 also exhibited a slight distortion in the early part of the energy return peak (Fig 4b). This irregularity has several potential causes: bone voids surrounding the implant, movement within the abutment/crown complex, or incomplete fractures in the veneering porcelain. Upon examination of the porcelain-fused-to-metal crown used to restore the implant, a small incomplete porcelain fracture was noted in the interproximal surface, but no movement was seen in the abutment/crown complex. Thus, it is possible that the early distortion in the energy return response (as represented by the depression in the ascending initial curve) could have resulted from this small fracture in the coronal superstructure or some hidden bony defect (Fig 4b).

The energy return response for site 14 appeared at first to be normal (Fig 4c). Closer examination revealed a small additional peak late in the energy response. This late peak

extended the time needed to complete the percussion response. The late timing of this additional peak could be related to a local instability at the bone level, as opposed to movement in the coronal region. Upon examination, there was no movement in the coronal region. However, the corresponding energy return curves and the average cortical bone plot for site 14 in Figs 4c and 5c illustrates that site 14 gave an irregular percussion probe response and had almost no crestal cortical bone support, with moderate to good cortical bone support at the apex. Figure 2c again confirmed that site 14 lacked cortical bone support at the crest (unstable crest), but the apical CT scans showed good cortical bone support at the apex (stable apex).

The energy return data for site 22 can also be compared with the average cortical bone density plot in Figs 4d and 5d. The results indicate that site 22 exhibited the highest level of instability in the present study based on the NFE from percussion data. CT data shown in Fig 2d revealed a significant lack of cortical bone in the crestal (unstable crest) and the apical (unstable apex) regions. This substantial instability is graphically illustrated in Figs 4d and 8, which revealed that site 22 exhibited the highest NFE of all 11 implants tested.

The present results indicate that cortical bone support, particularly at the apex and crest, is correlated with the level of functional stability of an implant under dynamic loading. The comparative analysis of the energy return peaks and the average percent cortical bone were found to be consistent and related. The Student *t* test was applied to linear regression of NFE plotted against overall relative bone density (Fig 3), NFE vs. average percent cortical bone (Fig 7), and NFE against cortical bone percentage at the crest and apex only (Fig 8). A *P* value of .305 indicated no statistically significant correlation between the average relative bone density and NFE. In Fig 7, the *P* value for the cortical bone correlation was .0609, which depicted a much more significant correlation than that between the average relative bone density and NFE. By further contrast, the *P* value of .0098 for the cortical bone correlations in Fig 8 was less than .05, indicating that it showed the most statistically significant correlation between crestal and apical cortical bone property and NFE. This finding is consistent with the results of Tuukkanen et al,[29] who showed that osteopenic bone in rat femurs, which contains less cortical bone but a greater overall mineral density, is significantly weaker than the normal rat femur. A somewhat lower *P* value and greater correlation coefficient in Fig 8 compared to those in Fig 7 suggest that the crestal and apical cortical bone have a greater influence on the stability of an implant. These results support the hypothesis that defects at or near the crest and the apex of an implant will cause it to be unstable and that this instability can be detected using percussion probe diagnostics. The stability of the implant determines its response to forces generated by mastication and parafunctional loading, which can also affect the level of osseointegration.

It is worth noting that the largest difference in apical/crestal cortical bone density between neighboring data points in Fig 8 was that between values for implant sites 14 and 34, despite relatively close NFE values. Their energy return response data in Fig 4 shows that the deviation in the response for site 34 from a symmetric bell-shaped peak was relatively early in the response (< 0.1 ms). By contrast, this deviation for site 14 occured at around 0.3 ms, with the appearance of an additional peak in the response. These observations suggest that the temporal position of the deviation from a normal response, in addition to the overall

NFE, is indicative of the severity of the corresponding defect in the structure. Further work is needed to explore this possibility for improving the analysis and interpretation of the percussion data.

Conclusion

Analysis of a human subject pre- and postmortem indicates that quantitative percussion data are indicative of the amount of dense cortical bone surrounding the subject's 11 implants located throughout the maxilla and mandible. Normal fit error values determined from percussion energy return data correlated with cortical bone supporting each implant and more significantly with the amount of cortical bone support at the apical and crestal regions of each implant. The normal fit error may provide clinicians with another diagnostic indication to assess the stability of dental implants, helping to quantify an individual implant's level of osseointegration.

Acknowledgement

The authors would like to thank the American Equilibration Society for their generous support of this work. The authors wish to also thank Hytec Inc. in Los Alamos, New Mexico, for the use of their model FCT2252 CT scanner, as well as Prof. Eric Herbranson, Prof. Joerg Meyer, Dr. Lawrence Lorenzi, Dr. Robert Fontanesi, and Dr. Paul Brown for their helpful assistance. The statistical analysis described was supported by the National Center for Research Resources and the National Center for Advancing Translational Sciences, National Institutes of Health (grant UL1 TR000153). The content is solely the responsibility of the authors and does not necessarily represent the official views of the National Institutes of Health. Assistance with this analysis from Dr. Robert Newcomb is gratefully acknowledged. The authors reported no conflict of interest related to this study.

Appendix A

The force variation resulting from Periometer percussion is determined by a sensor in the handpiece.[7] The energy return, E_r, characterizes the elastic energy of this force:

$$E_r = \frac{F^2}{2k} \quad \text{(A1)}$$

where F is the resultant percussion force and k is the stiffness of the percussion rod assembly. The normalized energy return is the energy return during impact divided by the kinetic energy of the percussion rod just prior to impact with the sample. It was found that the energy return/impact energy variation for a defect-free calibration sample could be expressed in the form:

$$\bar{E}_r = \beta \sin^2(\gamma t) \exp\left[\frac{(t-\phi)^2}{\psi}\right] \quad \text{(A2)}$$

where t is time, and β, γ, φ, *and* ψ are parameters that are determined by the best fit to the experimental data.

A nonlinear regression fit of equation A2 to 10 energy return data sets was performed for each implant model in the present study using the Levenberg-Marquardt algorithm.[19] The resulting mean residue, weighted mean error of the fitted model to all 10 data sets, was divided by the amplitude of the fit to the data to obtain NFE. This normalization of the mean

fit error with the amplitude is justified by the observation that defects have a greater effect on distorting energy return peaks that have higher amplitudes. It is also reasonable that a greater distortion in the mechanical response results when more energy is available to drive the movements associated with a defect.

References

1. Skalak, R. Introduction to Osseointegration. In: Brånemark, PI.; Zarb, G.; Albrektsson, T., editors. Tissue-Integrated Prosthesis: Osseointegration in Clinical Dentistry. Chicago: Quintessence; 1987. p. 117-128.
2. Brånemark R, Brånemark PI, Rydevik B, Myers RR. Osseointegration in skeletal reconstruction and rehabilitation. J Rehabil Res Dev. 2001; 38(2):175–181. [PubMed: 11392650]
3. Sheets CG, Earthman JC. Tooth intrusion in implant-assisted prostheses. J Prosthet Dent. 1997; 77(4):39–45. [PubMed: 9029464]
4. Sheets CG, Earthman JC. Natural tooth intrusion and reversal in implant-assisted prosthesis: Evidence of and a hypothesis for the occurrence. J Prosthet Dent. 1993; 70(6):513–520. [PubMed: 8277440]
5. Torzilli PA, Burstein AH, Takebe K, Zika JC, Heiple KG. The material properties of immature bone. J Biomech Eng. 1982; 104(1):12–20. [PubMed: 7078113]
6. VanSchoiack LR, Wu JC, Sheets CG, Earthman JC. Effect of bone density on the damping behavior of dental implants: an in vitro method. Mater Sci Eng. 2006; 26(8):1307–1311.
7. Meredith N, Alleyne D, Cawley P. Quantitative determination of the stability of the implant-tissue interface using resonance frequency analysis. Clin Oral Implant Res. 1996; 7(3):261–267.
8. Sennerby L, Meredith N. Resonance Frequency Analysis: Measuring implant stability and osseointegration. Compend Contin Educ Dent. 1998; 19(5):493–502. [PubMed: 9693511]
9. Magne P, Silva M, Oderich E, Boff LL, Encisco R. Damping behavior of implant-supported restorations. Clin Oral Implants Res. 2013; 24(2):143–148. [PubMed: 22092518]
10. Lazan, BJ. Damping of Materials and Members in Structural Mechanics. New York: Pergamon Press; 1968.
11. Winkler S, Morris HE, Spray JR. Stability of implants and natural teeth as determined by the Periotest over 60 months of function. J Oral Implantol. 2001; 27(4):198–203. [PubMed: 12500879]
12. Faulkner MG, Wolfaardt JF, Chan A. Measuring abutment/implant joint integrity with the Periotest instrument. Int Oral Maxillofac Implants. 1999; 14(5):681–688.
13. Magne P, Belser U. Rationalization of shape and related stress distribution in posterior teeth: a finite element study using nonlinear contact analysis. Int J Periodontics Restorative Dent. 2001; 22:425–433. [PubMed: 12449302]
14. Elias JJ, Brunski JB, Scarton HA. A dynamic modal testing technique for noninvasive assessment of bone-dental implant interfaces. Int Journal Oral Maxillofac Implants. 1996; 11(6):728–734.
15. Earthman, JC., inventor; Earthman, JC.; Sheets, CG., assignees. System and method for quantitative measurements of energy damping capacity. US Patent. 6,120,466. 2000 Sep 19. 2006
16. Earthman, JC.; Sheets, CG., inventors. Evaluation of reflected time-energy profile for determination of damping capacity. US Patent. 6,997,887. 2006. Feb 14.
17. Earthman, JC.; Sheets, CG., inventors. Evaluation of reflected time-energy profile for evaluating osseointegration and density. US Patent. 7,008,385. 2006. Mar 7.
18. Meyer J, Earthman JC, Sheets CG. Visualization of osseointegration of maxilla and mandible dental implants. Int J Comput Assist Radiol Surg. 2009; 5:59–76.
19. Nocedal, J.; Wright, SJ. Numerical Optimization. ed 2. New York: Springer; 2006.
20. Papavero L, Zwonitzer R, Burkard I, Klose K, Herrmann HD. A composite bone graft substitute for anterior cervical fusion: Assessment of osseointegration by quantitative computed tomography. Spine. 2002; 27(10):1037–1043. [PubMed: 12004170]

21. Wang X, Meier D, Taguchi K, et al. Material separation in x-ray CT with energy resolved photoncounting detectors. Med Phys. 2011; 38(3):1534–1546. [PubMed: 21520865]
22. Manjunatha HC, Rudraswamv B. Computation of CT-number and Z(eff) in teeth. Health Phys. 2011; 2:92–99.
23. Kouznetsov A, Tambasco M. A hybrid approach for rapid, accurate, and direct kilovoltage radiation dose calculations in CT voxel space. Med Phys. 2011; 38(3):1378–1388. [PubMed: 21520849]
24. Devlin H, Horner K, Ledgerton D. A comparison of maxillary and mandibular bone mineral densities. J Prosthet Dent. 1998; 79(3):323–327. [PubMed: 9553887]
25. Wowern N. Variations in bone mass and bone activity within the mandible. Calcif Tissue Int. 1975; 21:397–404.
26. De Maeseneer M, De Wilde V, Gosselin R, Oseaux M. The use of phantoms or tissue simulating test objects in the evaluation of imaging methods. JBR-BTR. 2003 Jan-Mar;86(10):3–5. [PubMed: 12675492]
27. Bouxsein ML, Boyd SK, Christiansen BA, Guldberg RE, Jepsen KJ, Müller R. Guidelines for assessment of bone microstructure in rodents using micro-computed tomography. J Bone Miner Res. 2010 Jul; 25(7):1468–1486. [PubMed: 20533309]
28. Loubele M, Maes F, Schutyser F, Marchal G, Jacobs R, Suetens P. Assessment of bone segmentation quality of cone-beam CT versus multislice spiral CT: A pilot study. Oral Surg Oral Med Oral Pathol Oral Radiol Endod. 2006 Aug; 102(2):225–234. [PubMed: 16876067]
29. Tuukkanen J, Koivnangas A, Jämsä T, Sunquist K, MacKay CA, Marks SC Jr. Mineral density and bone strength are dissociated in long bones of rat osteopetrotic mutations. J Bone Miner Res. 2000; 15910:1905–1911. [PubMed: 11028442]

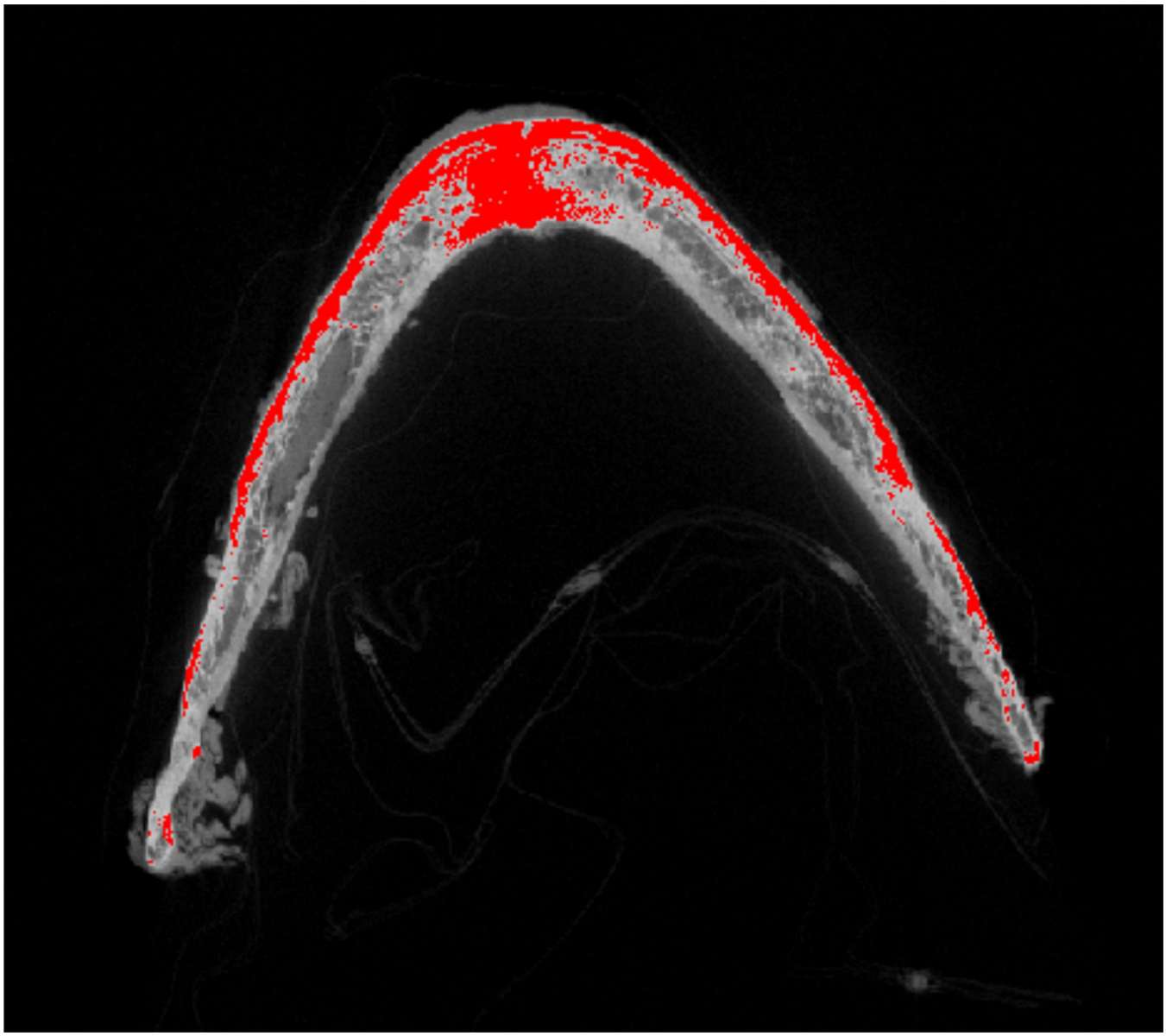

Fig 1.
An illustration of the detection of the highest density cortical bone at the inferior border of the subject's mandible *(red regions)*.

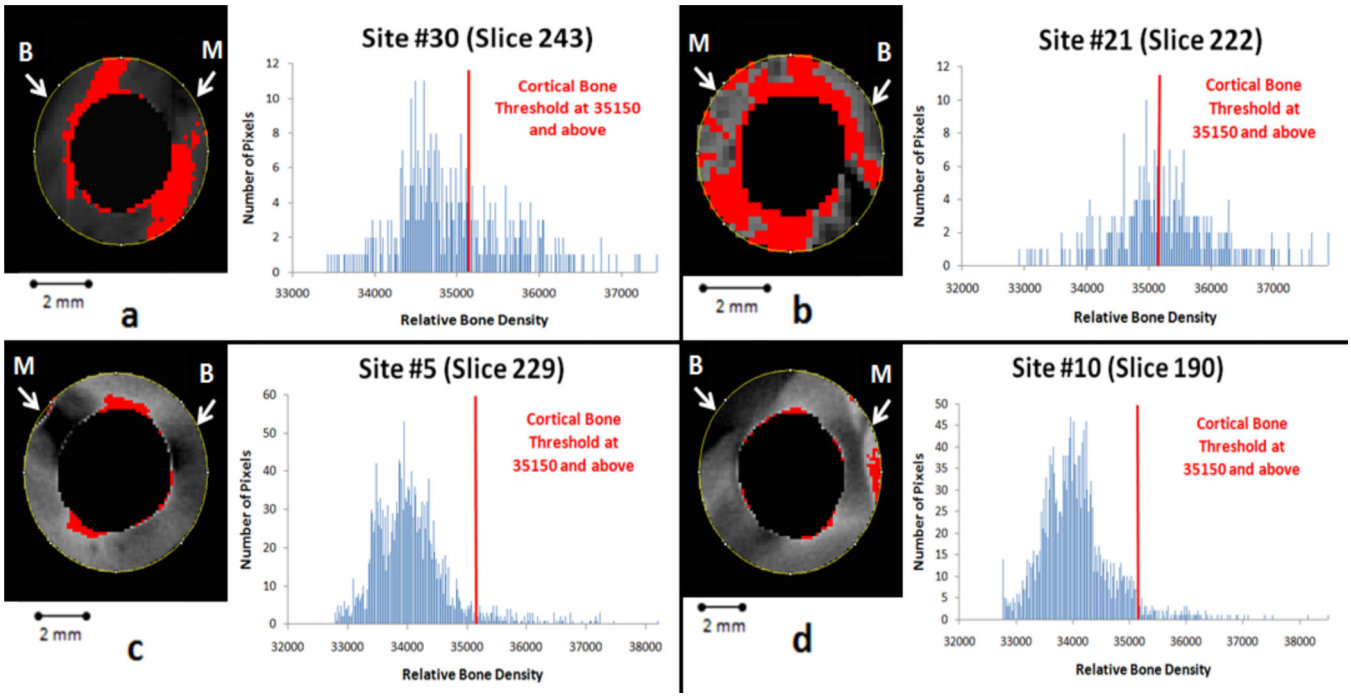

Fig 2.

CT scans and corresponding histograms near the implant crest for the *(a)* mandibular right first molar, *(b)* mandibular left first premolar, *(c)* maxillary right first premolar, and *(d)* maxillary left lateral incisor sites. RBD = relative bone density; B = buccal; M = mesial.

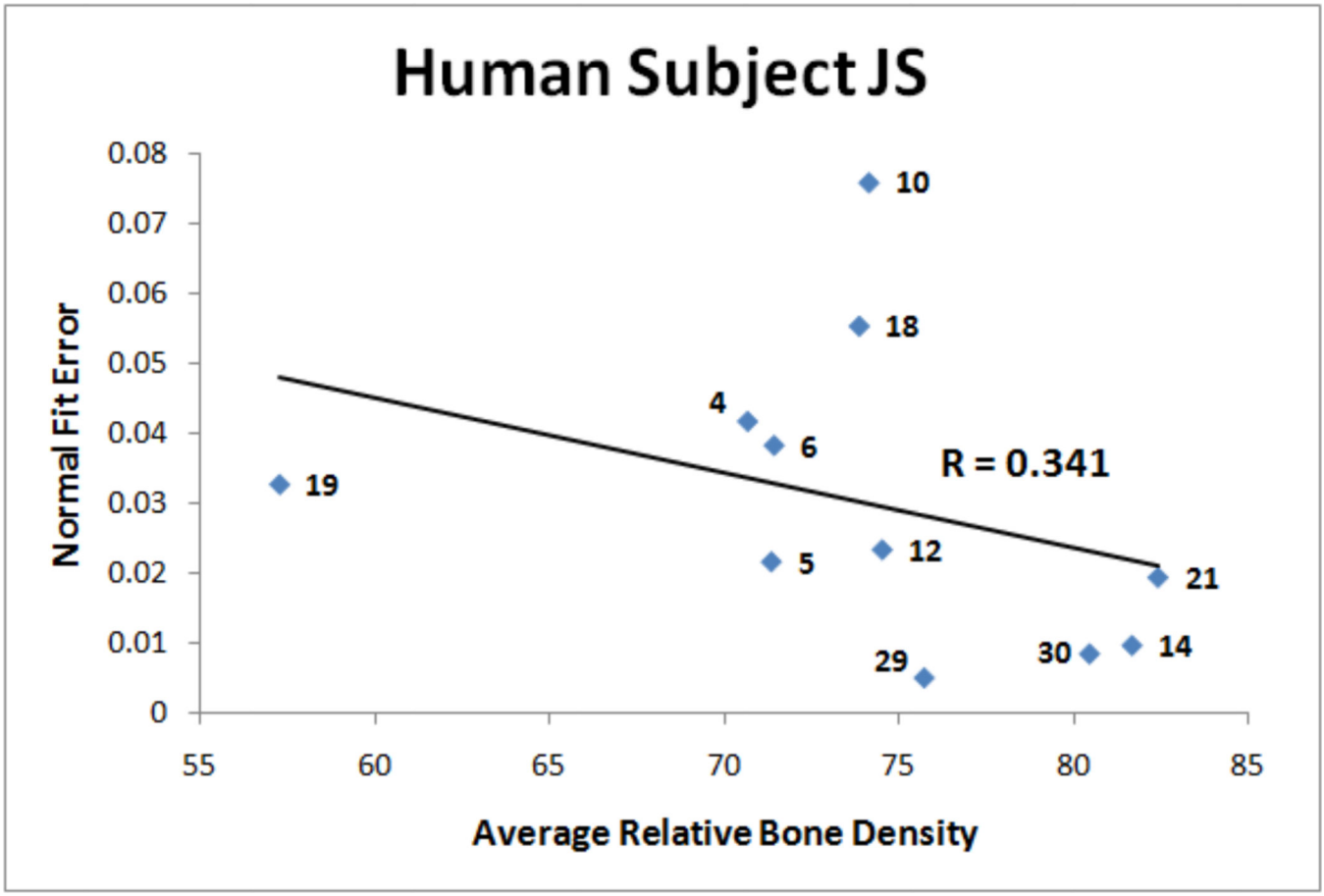

Fig 3.
NFE versus the average relative bone density (RBD) for each implant tested.

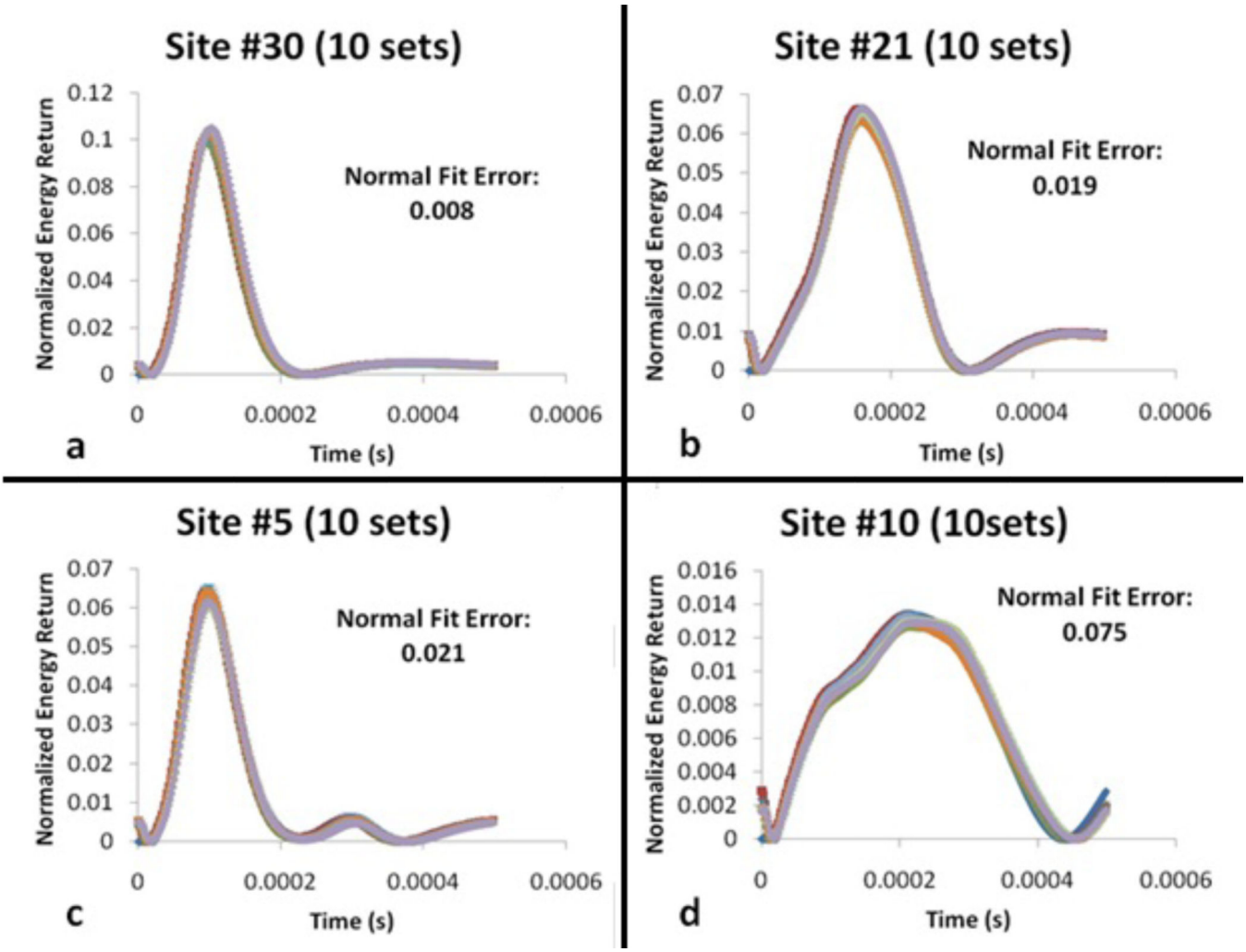

Fig 4.

Normalized energy return as a function of time for the *(a)* mandibular right first molar, *(b)* mandibular left first premolar, *(c)* maxillary right first premolar, and *(d)* maxillary left lateral incisor sites.

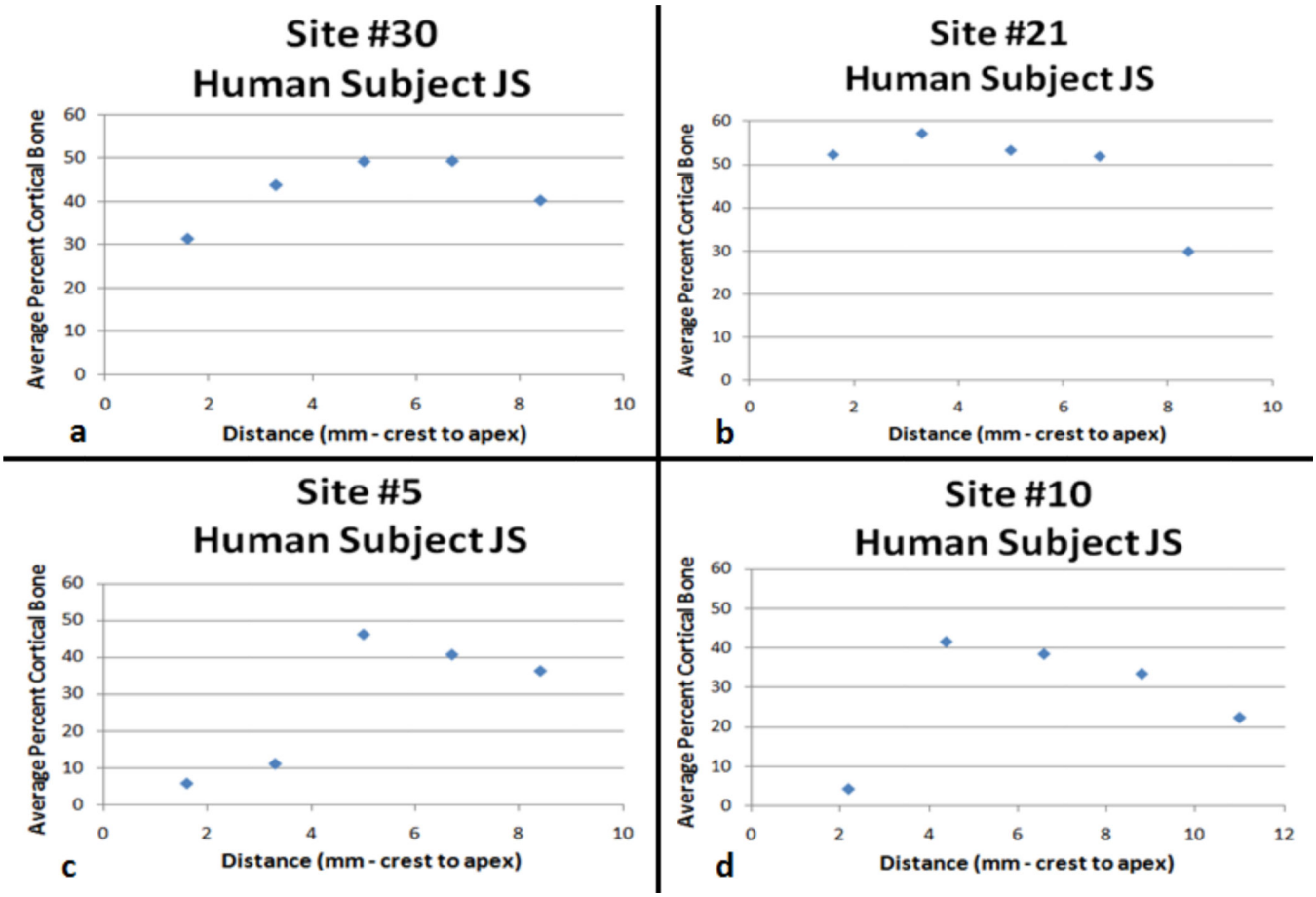

Fig 5.

Average percent cortical bone as function of distance along the implant for the (a) mandibular right first molar, (b) mandibular left first premolar, (c) maxillary right first premolar, and (d) maxillary left lateral incisor sites.

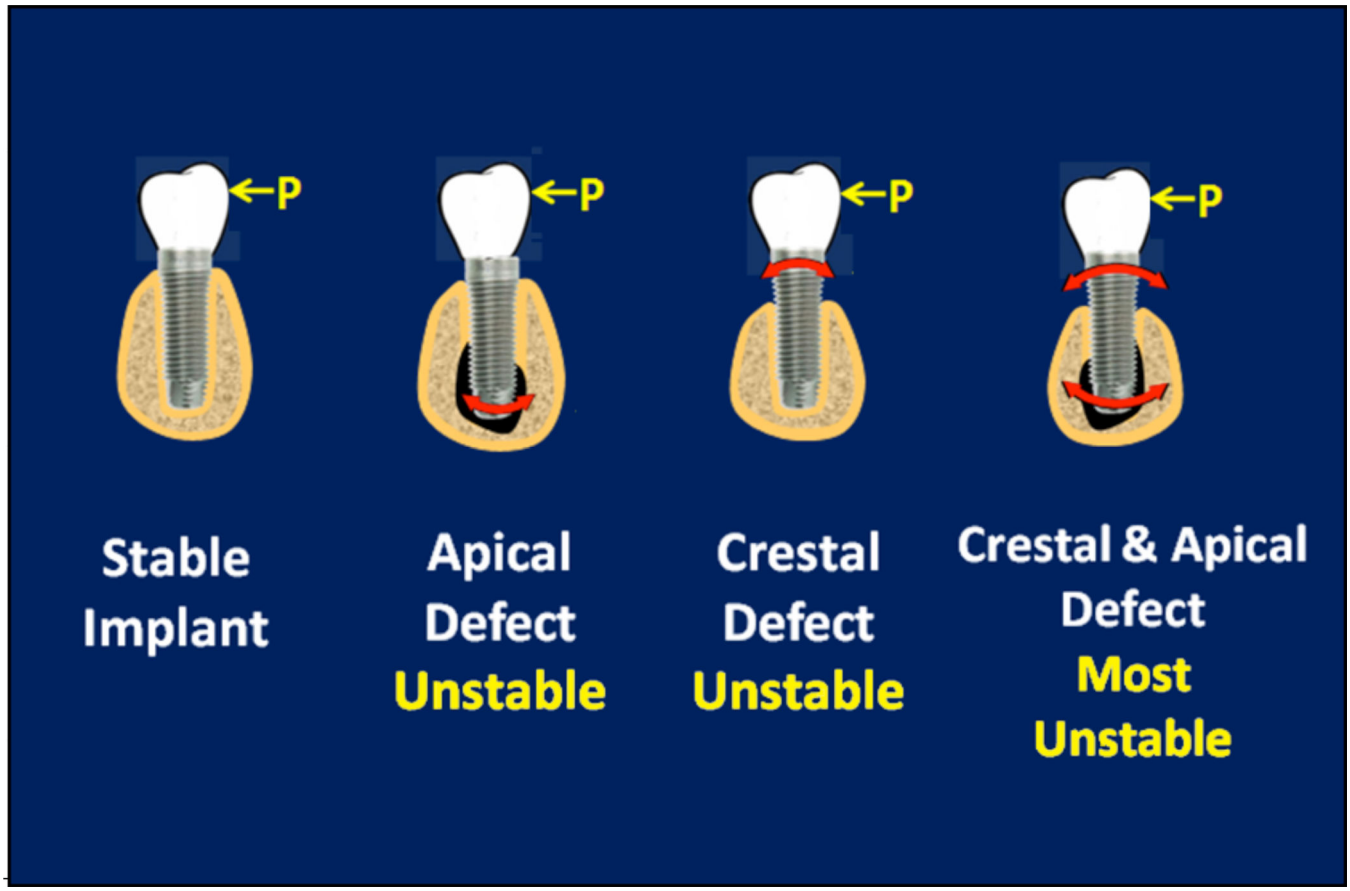

Fig 6.

Schematic that illustrates the behavior of implants with differing qualities of bone support. The symbol “P” indicates the direction of percussion on each superstructure.

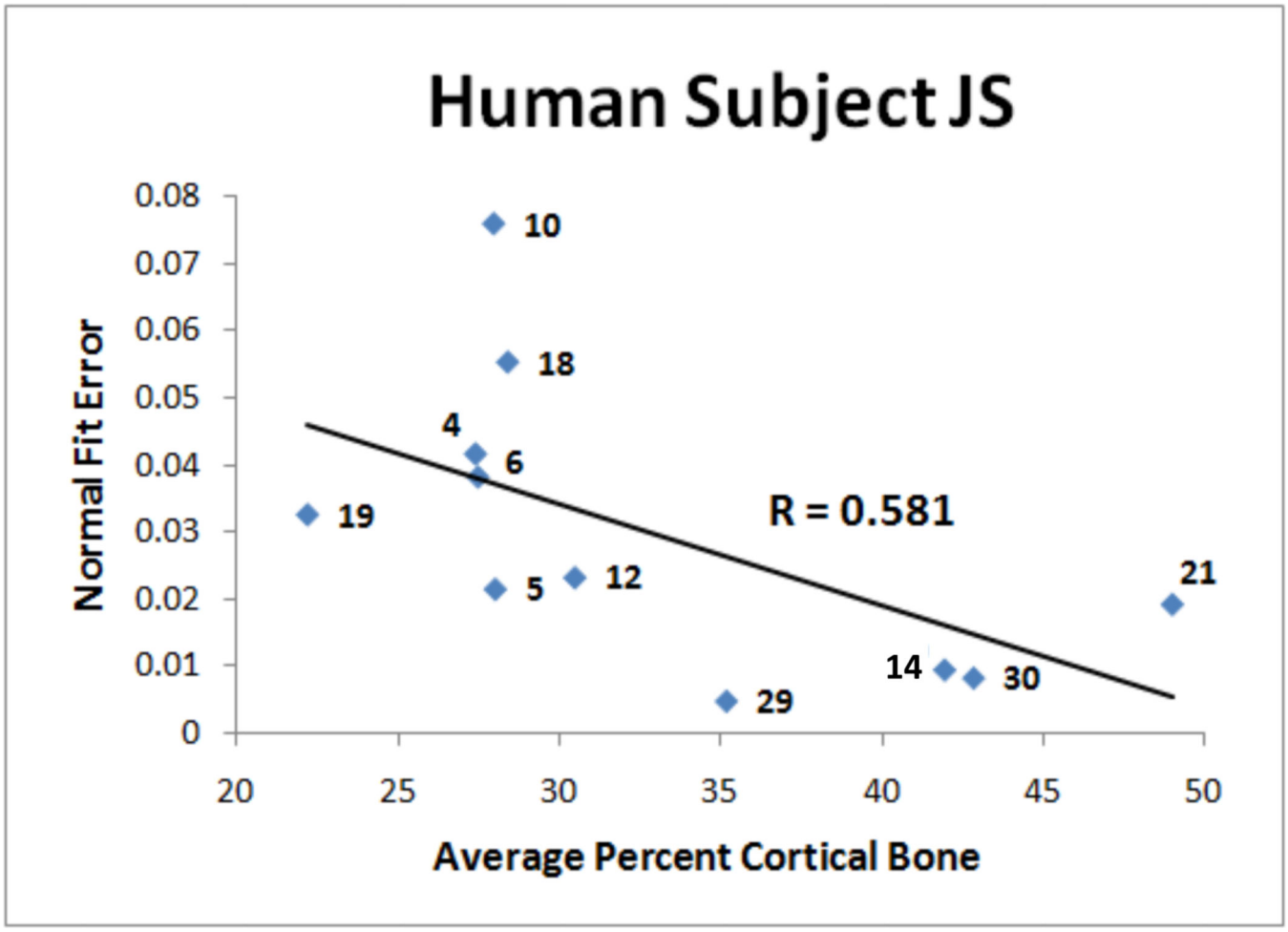

Fig 7.
NFE plotted against the average percent cortical bone supporting each implant.

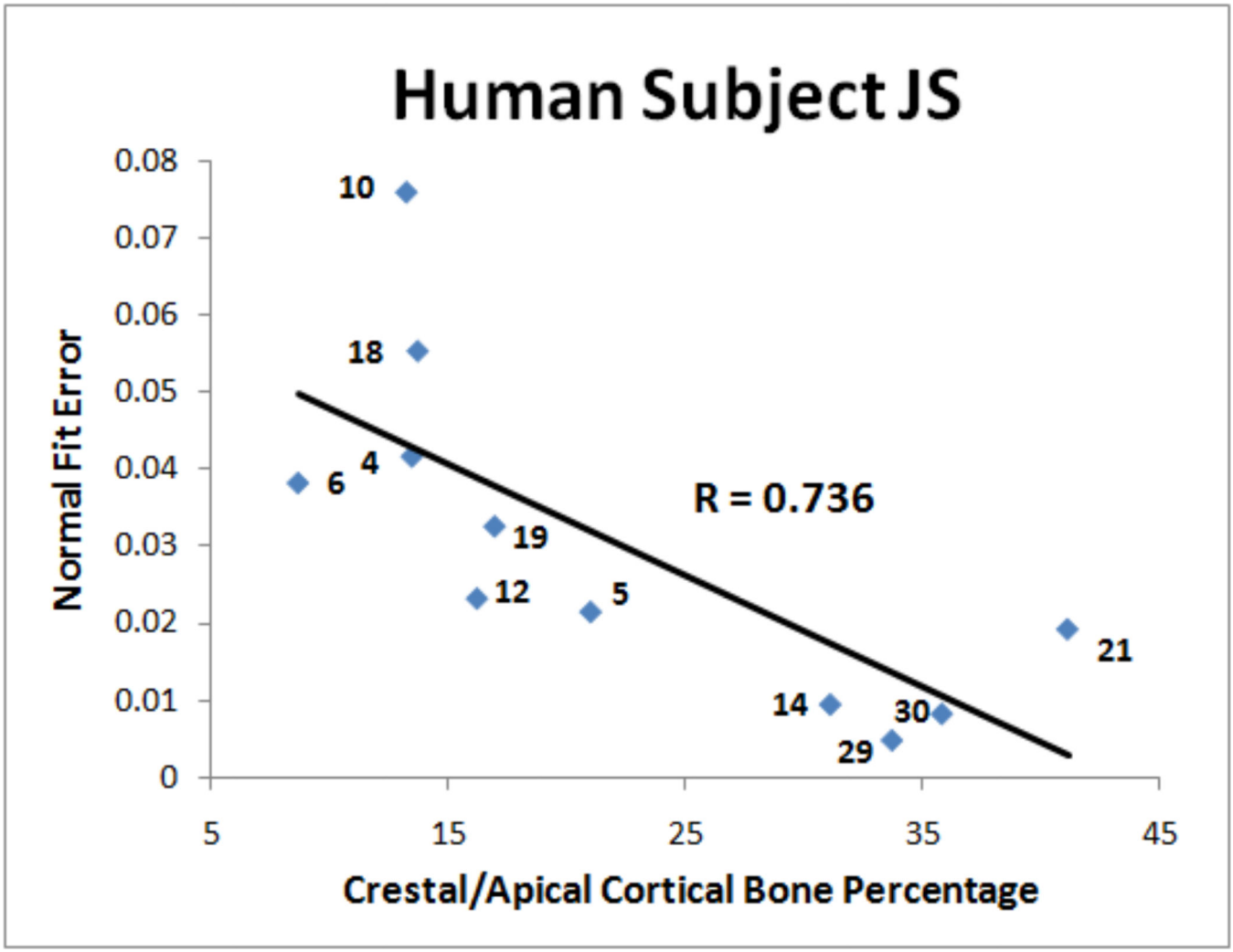

Fig 8.

NFE plotted against the average percent cortical bone in the crestal and apical regions for each implant.